Purity of Vector Vortex Beams through a Birefringent Amplifier

Hend Sroor,[1] Nyameko Lisa,[1,2] Darryl Naidoo,[1,2] Igor Litvin,[2] and Andrew Forbes[1,*]
[1]School of Physics, University of the Witwatersrand, Private Bag 3, Wits 2050, South Africa
[2]CSIR National Laser Centre, P.O. Box 395, Pretoria 0001, South Africa

(Received 8 November 2017; revised manuscript received 2 March 2018; published 6 April 2018)

Creating high-quality vector vortex (VV) beams is possible with a myriad of techniques at low power, and while a few studies have produced such beams at high power, none have considered the impact of amplification on the vector purity. Here we employ tools to study the amplification of VV beams and, in particular, the purity of such modes. We outline a versatile toolbox for such investigations and demonstrate its use in the general case of VV beams through a birefringent gain medium. Intriguingly, we show that it is possible to enhance the purity of such beams during amplification, paving the way for high-brightness VV beams, a requirement for their use in high-power applications such as optical communication and laser-enabled manufacturing.

DOI: 10.1103/PhysRevApplied.9.044010

I. INTRODUCTION

Laser modes with spatially inhomogenous polarization states, so-called Poincaré sphere beams, are highly topical of late [1]. One example of such beams is the well-known cylindrical vector vortex (CVV) beams [2–4]. They are characterized by a doughnutlike intensity distribution about a polarization singularity and are represented by a point on the higher-order Poincaré sphere (HOPS) [5,6] as shown in Fig. 1(a). Here the poles are scalar circularly polarized orbital angular momentum (OAM) modes with an azimuthally dependent phase of $\exp(\pm i\ell\phi)$, where ℓ is the topological charge and ϕ is the azimuthal angle, while the CVV beams are found on the equator: radially and azimuthally polarized beams, as well as the two hybrid states, together forming the waveguide modes.

Creating such beams has become commonplace in modern laboratories [7–17], and as a result they have found many applications: They form tighter focal spots than diffraction-limited beams, which makes them suitable for stimulated emission depletion superresolution microscopy applications [18], while the unique reduced scattering of the photons at the beam vortex makes such beams more desirable in optical trapping and tweezing of smaller-size particles [19] such as ultracold atoms and Bose-Einstein condensates. In optical communication, in free space and fiber, such modes provide a new degree of freedom (channels) in which information can be encoded [4,20–24]. More pertinently, there is a need for high-power CVV beams in laser-enabled manufacturing, where vector vortex modes are preferred due to their unique, nonuniform polarization patterns and tighter focusing that provide superior quality in drilling, welding, and cutting [25–29]. To address this, CVV beam amplification has become a topic of current research but with only limited studies to date that considered the output power of CVV beams from isotropic amplifiers [30–32].

While the output power achievements are well documented [30–32], the vector purity, a measure of the degree to which a beam is nonseparable in polarization and spatial degree of freedom, akin to the degree of polarization of a field, remains unstudied. It is self-evident that if the vector nature is needed in a particular application, for example, radially polarized light in laser materials processing or azimuthally polarized light for optical trapping and tweezing, then the vector quality (purity) will play a significant role in the efficacy of the beam for that application. Thus, we ask the question: How does the vector purity of the VV beam change with amplification? Analogous to scalar beams, where amplification tends to increase the power at the expense of the mode quality, here we consider if the vector quality likewise changes during amplification.

To address this, we outline an approach to studying the amplification of vector beams, in general, and CVV beams, in particular. We concentrate on the detection and quantification of the purity of such beams and demonstrate the approach by considering the general case of VV beams through a birefringent gain medium. We experimentally demonstrate the impact that the amplification process has on such beams and highlight an intriguing outcome, namely, that it is possible to increase not only the power but also the purity of the amplified mode by a judicious choice of gain. This suggests a route to high-brightness vector beams where power and quality are simultaneously increased.

II. THEORY

We wish to understand how the amplification process affects the vector purity of a vector beam. To do this, we

*andrew.forbes@wits.ac.za

first introduce a definition of purity, a toolbox to measure it, and then proceed to consider the impact of amplification on the purity. As CVV beams have been shown to have many applications, we begin with such beams but quickly generalize the results to arbitrary modes. To begin, let us consider a HOPS beam of the form

$$U(r,\phi) = \sqrt{\alpha}\exp(i\ell\phi)\hat{\mathbf{e}}_{\mathbf{R}} + \exp(i\gamma)\sqrt{1-\alpha}\exp(-i\ell\phi)\hat{\mathbf{e}}_{\mathbf{L}}, \tag{1}$$

where the vectors $\hat{\mathbf{e}}_{\mathbf{R}}$ and $\hat{\mathbf{e}}_{\mathbf{L}}$ are the right-circular and left-circular polarization states, respectively, and γ is an intramodal phase. For example, when $\alpha = 0.5$ we have our CVV beams: For $\gamma = 0$ we have radially polarized light, while for $\gamma = \pi$ we have azimuthally polarized light, both of which have found many applications as indicated earlier; e.g., radially polarized light is twice as efficient as compared to circularly polarized light in laser materials processing [26], while pure azimuthally polarized light has a sharper focal spot for more efficient optical trapping and tweezing [18]. Of course, when $\alpha = 1$ or 0, the beam is scalar and clearly then partially vector for intermediate states.

How should one define the vector purity to reflect this? We elect to draw on the similarities between entangled quantum states and classical vector states, both sharing the property of nonseparability. Indeed, this is the quintessential property of entangled systems with the classical analogue sometimes referred to as classical entanglement [33–39] and, beyond a purely mathematical analogy, has been shown to have physical significance [40]. Applying quantum tools to our vector modes allows us to quantify their vector purity, since vector purity is precisely the degree of nonseparability of the mode [41,42]. This allows one to calculate a vector quality factor (VQF) for a beam of the form given by Eq. (1), a quantitative measure of the vector purity, which may be expressed as (see the Appendix and Ref. [41])

$$V = 2|\sqrt{\alpha(1-\alpha)}|, \tag{2}$$

with the range of 0 (scalar) through 1 (vector). Thus, the parameter α defines the transverse mode structure, from purely scalar ($\alpha = 1$ or 0) to purely vector ($\alpha = 0.5$); otherwise, it is partially vector, while the phase (γ) only produces a rotation and thus does not affect vector purity. For this reason, we neglect it in the rest of this treatment. Note that this is a special form of the factor V for the case of the state given by Eq. (1), which we shortly generalize to arbitrary modes. Nevertheless, it is general in the sense that Eq. (1) describes any HOPS beam, from CVV beams to circularly polarized OAM beams, and thus Eqs. (1) and (2) describe our initial beam to be amplified as well as the initial purity. It is more convenient to express the polarization vectors in terms of horizontal and vertical states $\hat{\mathbf{e}}_{\mathbf{H}}$ and $\hat{\mathbf{e}}_{\mathbf{V}}$, respectively, which we do from now on in the notation. Strictly speaking, this removes the cylindrical symmetry, so that the study is of a

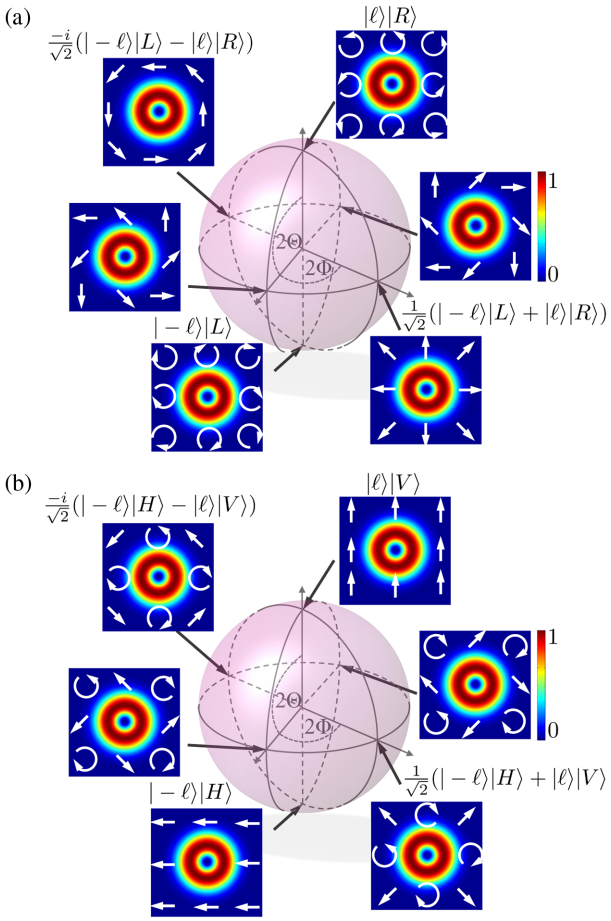

FIG. 1. Illustration of (a) a HOPS representing VV modes in the left and right polarization basis and (b) a modified HOPS representing the VV modes in the horizontal and vertical basis. The output beam profile is displayed at different positions on the sphere with arrows indicating polarization distribution.

more general OAM VV beam represented by a point on the modified HOPS shown in Fig. 1(b). Our beam is then

$$U(r,\phi) = \sqrt{\alpha}\exp(i\ell\phi)\hat{\mathbf{e}}_{\mathbf{H}} + \sqrt{1-\alpha}\exp(-i\ell\phi)\hat{\mathbf{e}}_{\mathbf{V}}. \tag{3}$$

When such a beam is passed through an amplifier, the input field transforms to an output field given by

$$\tilde{U} = \begin{pmatrix} \tilde{U}_h \\ \tilde{U}_v \end{pmatrix} = \begin{pmatrix} a_1\exp(i\ell\phi) + a_3\exp(-i\ell\phi) \\ a_2\exp(i\ell\phi) + a_4\exp(-i\ell\phi) \end{pmatrix}, \tag{4}$$

where we write the field with the Jones matrix formalism in the horizontal-vertical basis, with a new VQF given by (see the Appendix)

$$V = \frac{2|a_1a_4 - a_2a_3|}{a_1^2 + a_2^2 + a_3^2 + a_4^2}. \tag{5}$$

Here we have a more general form of Eq. (1), with four terms, which can be made completely general by making

the substitution from OAM modes to general modes M_h and M_v, i.e., $\exp(i\ell\phi) \to M_h$ and $\exp(-i\ell\phi) \to M_v$ in Eq. (4). Note that the calculation of the purity of the mode [Eq. (5)] is not affected by this change. This is because the purity V is based on how separable the modes are and not what the modes look like that you are trying to separate. In the language of quantum mechanics, a Bell state is maximally entangled regardless of the degree of freedom you express it in. Thus, with the substitution just mentioned, Eqs. (4) and (5) are the general form of VV beams after some amplification stage (see comments later for a further generalization). The study here considers OAM VV beams due to their many applications as highlighted earlier.

Now we are in a position to understand the impact of the amplifier. Without any loss of generality, we imagine the case where the amplifier is oriented to have initial amplification factors η_{h0} and η_{v0} for horizontal and vertical polarization, respectively (defined at $\theta = 0$). Now when the crystal is rotated through an angle θ, the state alters and is uniquely determined from the coefficients (see the Appendix)

$$a_1 = \sqrt{\alpha}(\sqrt{\eta_{h0}}\cos^2\theta + \sqrt{\eta_{v0}}\sin^2\theta), \tag{6}$$

$$a_3 = \sqrt{1-\alpha}\cos\theta\sin\theta(\sqrt{\eta_{h0}} - \sqrt{\eta_{v0}}), \tag{7}$$

and

$$a_2 = \sqrt{\alpha}\cos\theta\sin\theta(\sqrt{\eta_{h0}} - \sqrt{\eta_{v0}}), \tag{8}$$

$$a_4 = \sqrt{1-\alpha}(\sqrt{\eta_{v0}}\cos^2\theta + \sqrt{\eta_{h0}}\sin^2\theta). \tag{9}$$

For isotropic amplifiers, the emission cross section is independent of polarization, so $\eta_{h0} = \eta_{v0} = \eta_0$. In this special case, the output vector state is identical to the input (purity remains the same) but with an increase in power, i.e., $\tilde{U} = \sqrt{\eta_0}U$.

In contrast, birefringent amplifiers generally have different emission cross sections for each polarization, and thus $\eta_{h0} \neq \eta_{v0}$. Here, each component of the vector state is amplified differently so that the vector nature (purity) itself changes along with the power content. Some examples of the effect of a birefringent amplifier are shown in Fig. 2, where the output purity V_{out} is plotted against the crystal rotation angle θ, the initial amplification ratio $\eta_R = \eta_{h0}/\eta_{v0}$ at $\theta = 0$, and α controls the input purity V_{in}.

We see that, when the input VV beam is pure ($V_{\text{in}} = 1$), the output vector purity is not a function of the crystal rotation angle and is always less than or equal to the input, as seen in the blue line in Fig. 2(a). This is understandable as a special case where the beam's polarization structure is rotationally symmetric and, thus, invariant to the crystal rotation. When $\alpha \neq 0.5$, this is no longer true, and we note that the vector purity may increase and/or decrease depending on the initial purity and amplification terms. For example, when the vertical component is initially larger and has higher amplification than the horizontal, shown in the orange curve in Fig. 2(a), the output purity is always less than the input. Conversely, when the vertical component is initially smaller than the horizontal but has higher amplification, the purity increases as the power weighting of the modes equalize (green curve). Note that whether or not the purity can be returned to $V_{\text{out}} = 1$ depends on the amplification ratio being sufficient to overcome the initial modal mismatch (in power weighting). This behavior is further explored in Figs. 2(b)–2(e).

When the initial state is symmetric in polarization or the amplification ratio is unity, then the purity is independent of the crystal angle, as shown in Figs. 2(b) and 2(e). However, when this is not the case, the purity can be increased to a maximum of $V_{\text{out}} = 1$ or decreased according to the parameters of the initial beam and the medium, illustrated in Figs. 2(c) and 2(d). It is this evolution in purity that we wish to uncover experimentally.

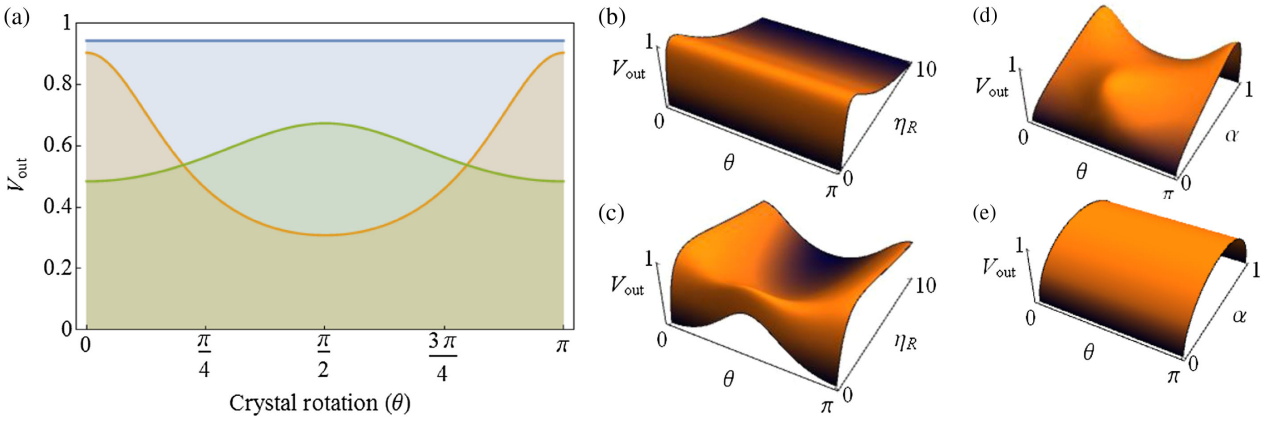

FIG. 2. (a) The vector quality factor V_{out}, as a function of crystal angle θ, for three cases: $\alpha = 0.5$ and $\eta_R = 2$ (blue), $\alpha = 0.8$ and $\eta_R = 0.1$ (orange), and $\alpha = 0.4$ and $\eta_R = 0.1$ (green). The 3D plots of the parameter space show the richness of the theory, with the input state fixed in (b) and (c) at $\alpha = 0.5$ and $\alpha = 0.7$, respectively. In (d) and (e), the amplification factor is fixed at $\eta_R = 0.2$ and $\eta_R = 1$, respectively.

III. EXPERIMENTAL SETUP

Our experiment is illustrated in Fig. 3. A horizontally polarized Gaussian beam is produced from a $\lambda = 1053$ nm continuous wave (cw) Nd:YLF laser source with an average power of approximately 164 mW. The beam polarization is adjusted (with Pol and QWP) and passed through a geometric phase element to create vector beams of variable purity. In this experiment, we create VV beams using a q plate, a birefringent wave plate with an azimuthally varying geometric phase [43–45]. The q plate performs spin (polarization) to orbit (our OAM mode) coupling following the ladder rules: $|\ell, L\rangle \rightarrow |\ell + 2q, R\rangle$ and $|\ell, R\rangle \rightarrow |\ell - 2q, L\rangle$, where q is the topological charge of the q plate (we use the Dirac notation for conciseness). Here, we exploit a q plate with $q = 1/2$ to produce VV beams with OAM modes of $\ell = \pm 1$. Our VV beam is passed through an amplifier comprising an uniaxial (birefringent) Nd:YLF crystal (6 mm diameter by 48 mm in length) which is end pumped by a 805-nm wavelength cw fiber coupled diode laser at 25 W of power. The crystal is mounted within copper blocks, maintained at 293 K by water cooling, with the c axis initially horizontal, thus defining the $\theta = 0$ position. Rather than rotate the crystal, which is cumbersome, we perform an identical experiment of rotating the initial beam relative to the crystal with the aid of a dove prism and a half wave plate (HWP3). Because the subsequent analysis of the beam is polarization sensitive, a second half wave plate (HWP4) and a dove prism are used to undo this rotation.

The VQF is found experimentally by performing a state tomography of the amplified beam, with full details given in the Appendix. This involves inner product measurements on each polarization component of the field with the six spatial projections given in Table I, i.e., the two OAM modes of $\exp(i\ell\phi)$ and $\exp(-i\ell\phi)$ and four superposition states given by $\exp(i\ell\phi) + \exp(i\delta)\exp(-i\ell\phi)$ with $\delta = 0$, $\pi/4$, $\pi/2$, and $3\pi/2$. Optically, the inner product is performed by directing the incident beam onto a holographic match filter and viewing the Fourier transform, with the use of a lens (FL), on a CCD camera [15]. Table I shows example holograms for each of these six projections, repeated for the incoming beam's two polarization components ($\tilde{U}_h$ and $\tilde{U}_v$), thus making 12 measurements in total and returning 12 real numbers, I_{ij} (i represents either 1 or 2 for the two polarization states and j is 1–6 for the spatial projections). For example, $I_{11} = |\langle \tilde{U}_h | \exp(i\ell\phi)\rangle|^2$ and $I_{23} = |\langle \tilde{U}_v | \exp(i\ell\phi) + \exp(-i\ell\phi)\rangle|^2$. The resulting Bloch vectors, akin to Stokes parameters, can then be calculated from these measurements using

TABLE I. The 12 projective measurements to find the unknown intensities I_{ij} for the calculation of the purity V.

	$\ell = 1$	$\ell = -1$	$\delta = 0$	$\delta = \pi/2$	$\delta = \pi$	$\delta = 3\pi/2$
						
$\tilde{U}_h$:	I_{11}	I_{12}	I_{13}	I_{14}	I_{15}	I_{16}
$\tilde{U}_v$:	I_{21}	I_{22}	I_{23}	I_{24}	I_{25}	I_{26}

$$
\begin{aligned}
S_1 &= (I_{13} + I_{23}) - (I_{15} + I_{25}),\\
S_2 &= (I_{14} + I_{24}) - (I_{16} + I_{26}),\\
S_3 &= (I_{11} + I_{21}) - (I_{12} + I_{22}),
\end{aligned}
\tag{10}
$$

from which the nonseparability of the beam, i.e., its vector purity (V), could be found from

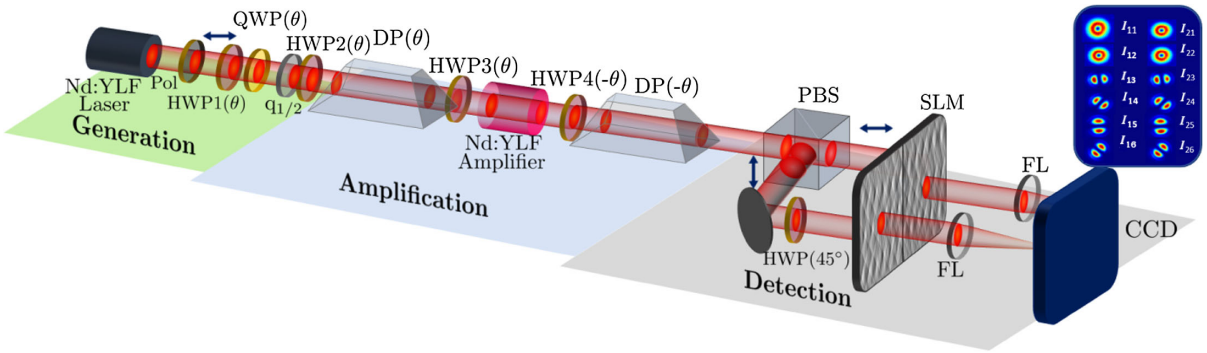

FIG. 3. The fundamental Gaussian mode of the source laser is modified in a generation step with a polarizer (Pol) and quarter wave plate (QWP) and passed through a q plate ($q_{1/2}$) to produce vector beams of variable purity, from 0 to 1. The resultant beam is passed through the amplification stage with half wave plates (HWP3 and HWP4) dove prisms (DP) on either side of the crystal gain medium in order to rotate the beam relative to the crystal axes (effectively rotating the crystal). Finally, the amplified beam is passed through a detection system to determine the VQF by a state tomography: After passing through a polarizing beam splitter (PBS), each component of the field is measured in the OAM basis by holograms encoded on a spatial light modulator (SLM). The outputs are measured in the Fourier plane using a charge-coupled device (CCD) camera.

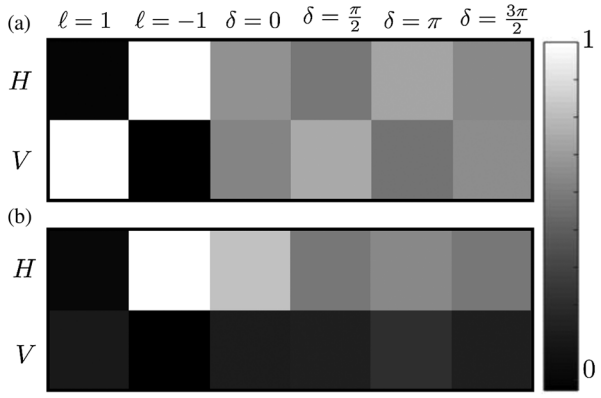

FIG. 4. Illustration of the actual intensity measurements I_{ij}, corresponding to (a) a perfect input VV beam with $V = 1$ and (b) an amplified VV beam with $V = 0.7$.

$$V = \mathrm{Re}\left(\sqrt{1 - \sum_{i=1}^{3} S_i^2}\right). \tag{11}$$

This is experimentally realized using a polarizing beam splitter (PBS) to spatially separate the horizontal and vertical polarization basis states which are directed toward an SLM encoded with the six OAM projections on a single hologram as shown in Fig. 3. By way of example, the results of the 12 projections for the seed and amplified beams for $\theta = 0$ are shown in Figs. 4(a) and 4(b), respectively.

IV. RESULTS

In order to calibrate the system and ensure correct operation, the purity of the input mode is altered by an adjustment of the QWP in Fig. 3 and measured with the detection system without any amplification ($\eta_{h0} = \eta_{v0} = 1$). The results confirm the system performance. Next, with the gain switched on, the amplification factors are measured as a function of the crystal orientation relative to the input beam. The experimental results are in good agreement with the theory, exhibiting oscillatory amplification as shown in Fig. 5.

This can be understood intuitively: At $\theta = \pi/2$, the input horizontal and vertical components appear swapped, and thus their amplification factors likewise interchange.

Next, a VV beam of $V = 1$ is amplified with the results shown in Fig. 6. As predicted by the theory, the purity of the mode is set by the initial amplification ratio and does not change when the crystal is rotated. In such a scenario, the purity of the initial mode can only *decrease* with amplification unless $\eta_R = 1$ (in which case it remains invariant). Conversely, the theory suggests that when the initial purity is not perfect, it is possible to increase or decrease the purity depending on the amplification ratio η_R. This is confirmed experimentally in Fig. 7(a).

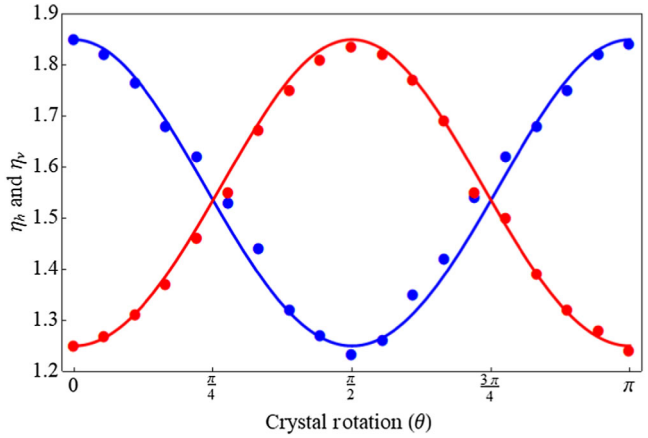

FIG. 5. Evolution of the horizontal and vertical amplification factors η_h (blue curve) and η_v (red curve) as a function of the orientation of the Nd:YLF crystal, θ. The points show the experimental data with the theoretical curves overlaid. The initial amplification factors at $\theta = 0$ are taken as our two parameters η_{h0} and η_{v0} for all calculations.

Here we select two initial beams, U_1 and U_2 from Eq. (3), with $\sqrt{\alpha} = 0.26$ and $\sqrt{\alpha} = 0.965$, respectively, so that both have identical initial purities of $V = 0.5$ before amplification. We observe the predicted oscillation in purity as a function of the crystal angle, illustrating that the purity could be improved from the initial value.

Clearly, the mechanism is partial equalization of the modal weightings in the VV beam. The amplitude of the oscillation is a function of both the initial purity and η_R, the available amplification ratio. This is illustrated on the modified HOPS in Fig. 7(b), showing how an

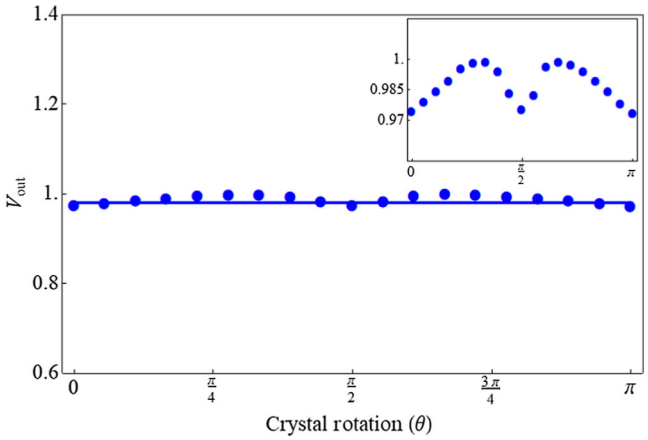

FIG. 6. Purity of the output beam over different orientations of the Nd:YLF amplifier for an input purity of $V = 1$. The theory is shown as the solid curve together with the experimental data points. The theory predicts $V = 0.99$ and independent of angle, which is corroborated by the experiment. The inset, an enlarged data sequence, shows a slight modulation due to a systematic experimental uncertainty in the form of rotation-dependent misalignment, an error on the order of 1%.

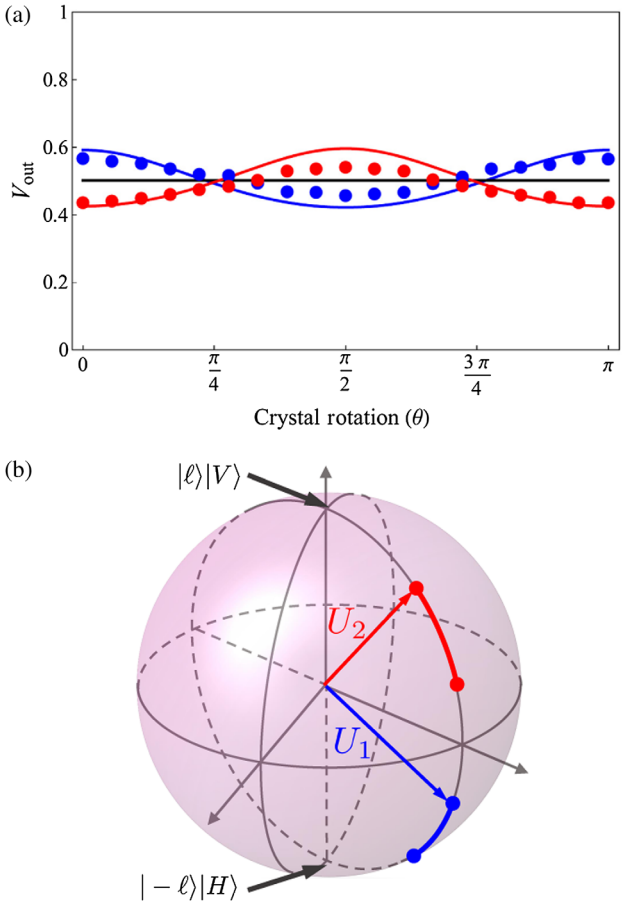

FIG. 7. (a) The vector purity of two VV beams, U_1 (blue) and U_2 (red), as the crystal axis is rotated (for identical $V_{in} = 0.5$). The purity oscillates about the initial value of 0.5 (black solid line) but in some cases is improved due to equalization of the modal weightings. (b) The same oscillation in purity is plotted on the HOPS as trajectories for the two beams, show in red and blue.

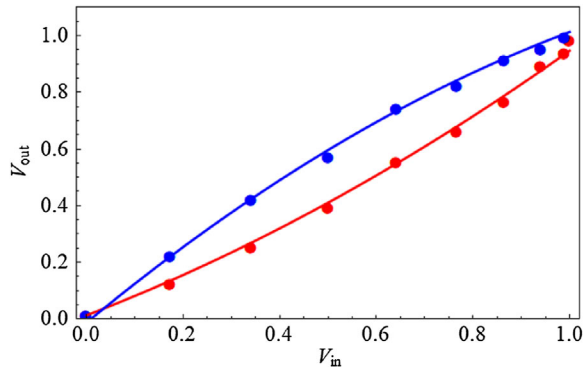

FIG. 8. The change in the purity of the amplified beam (V_{out}) with respect to the purity of the injected seed beam (V_{in}). By adjusting the QWP, the state of the input field continuously changes. The purity of the amplified beam V_{out} is calculated for QWP angle $\theta \in [0, 45]$ (blue dots) and $\theta \in [0, -45]$ (red dots). The experimental data are plotted against the theoretical predictions (solid lines), showing excellent agreement.

TABLE II. The adjustment of the QWP in order to change the purity of the initial state.

QWP (θ)	0°	5°	10°	15°	20°	25°	30°	35°	40°	45°
α	1.0	0.99	0.97	0.93	0.89	0.82	0.75	0.67	0.59	0.5
V	0.0	0.17	0.34	0.5	0.64	0.77	0.87	0.94	0.98	1.0

oscillation in purity affects the VV beam position on the sphere. Without any amplification, the beam with $V = 0.5$ is represented by a point on the sphere with $2\Theta = 60°$. After amplification, the position of VV beam U_2 (red) oscillates on the modified HOPS from $2\Theta \in [48°, 74°]$, while the position for VV beam U_1 (blue) oscillates $2\Theta \in [106°, 132°]$ as shown in Fig. 7(b). If the amplification ratio were tunable (see the discussion to follow), then it would be possible to increase the purity from any initial value to unity.

Finally, the purity V_{out} of the amplified beam is measured with respect to the input beam purity V_{in}, while the crystal is set at angle $\theta = 0$, with the results shown in Fig. 8. The input beam purity V_{in} is adjusted by continuously rotating the orientation of the QWP in Fig. 3 according to the settings summarized in Table II.

V. AMPLIFICATION OF CVV BEAMS

Next, we study the purity of cylindrical vector vortex (CVV) beams in the form of the four well-known waveguide modes: $|\mathrm{TM}\rangle$, $|\mathrm{TE}\rangle$, $|\mathrm{HE}_e\rangle$, and $|\mathrm{HE}_o\rangle$. These modes, which include radially and azimuthally polarized light fields, are generated by adjusting HWP1 and HWP2 in Fig. 3 according to Table III.

The seed CVV beams are amplified through the amplification stage as in Fig. 3, with the output of each following a trend in purity as of that in Fig. 6. To see how the purity changes with amplification, we measure the output power for each CVV beam as a function of the amplifier pump power, with the results shown in Fig. 9. At the threshold power of the amplifier (point A), the purity of the amplified CVV beam does not change (equal to the seed beam, $V = 1$). Well after the threshold point (point B), the purity

TABLE III. Required settings for HWP1, QWP, and HWP2 in order to generate pure $|\mathrm{TM}\rangle$, $|\mathrm{TE}\rangle$, $|\mathrm{HE}_e\rangle$, and $|\mathrm{HE}_o\rangle$ modes. The output CVV beam in each case would have a purity $V = 1$, as these are maximally nonseparable or ideal vector vortex beams.

Modes	$\|\mathrm{TM}\rangle$	$\|\mathrm{TE}\rangle$	$\|\mathrm{HE}_e\rangle$	$\|\mathrm{HE}_o\rangle$
	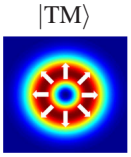	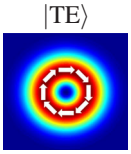	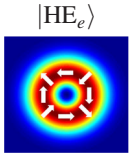	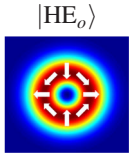
HWP1(θ)	0°	45°	0°	45°
QWP(θ)	45°	45°	45°	45°
HWP2(θ)	0°	0°	45°	45°

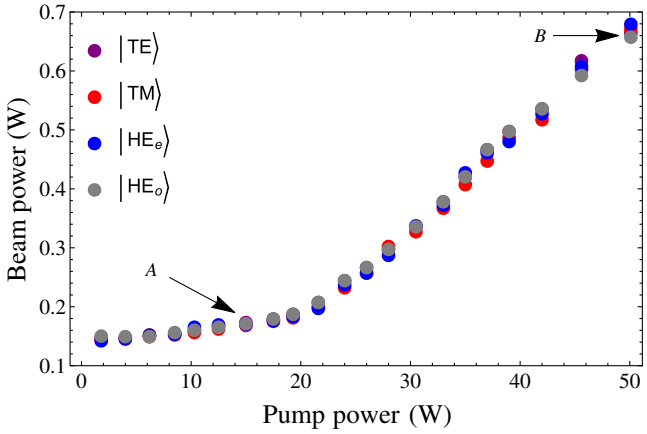

FIG. 9. The output power for the CVV beams as a function of the pump power for a given injected power of 164 mW. Point A represents the threshold point for the amplifier.

is measured to be $V = 0.988$ for $|\mathrm{TM}\rangle$, $V = 0.982$ for $|\mathrm{TE}\rangle$, $V = 0.986$ for $|\mathrm{HE}_e\rangle$, and $V = 0.983$ for $|\mathrm{HE}_o\rangle$. In other words, the purity of the modes is virtually unchanged.

VI. DISCUSSION AND CONCLUSION

The approach we outline here is general, with OAM modes used by way of example only. This is chosen partly due to the ease of creation of such modes and partly because of their topical nature in as far as applications are concerned. We explicitly select the horizontal and vertical basis so that symmetry does not cloud the general behavior. What we predict and observe is that the purity of vector modes is an important aspect to consider when amplifying such beams and that, in fact, the purity may be improved with a careful choice of parameters. For example, it will be possible by a sequence of crystals, judiciously rotated relative to one another, to overcome any degradation in purity due to the desired amplification. Although the measured output powers are in the range of < 1 W, we stress that this is a study on purity and not on optimizing the output power. We believe that this work provides an important platform for realizing high-brightness vector beams with high power and high purity. Finally, as we point out, a change of notation from OAM modes to general modes, i.e., $\exp(i\ell\phi) \to M_h$ and $\exp(-i\ell\phi) \to M_v$, will require only a change to the measurement holograms for the tomography without any change to the approach and theory. Similarly, while we study perturbations due to amplification, the approach outlined here can easily be adjusted to account for other vector perturbations such as polarization-dependent delivery systems, turbulence, and so on.

In conclusion, we introduce an approach with which to study the amplification of vector beams. We show the impact of birefringent gain on vector purity with nonbirefringent gain a special case of our results. We provide the theory and measurement toolbox for practical use and confirm its validity through an experiment under a range of conditions. Importantly, our results highlight a road map towards high-brightness vector beams, a core requirement for applications such as laser-enabled manufacturing and long-distance optical communication in free space and fiber.

ACKNOWLEDGMENTS

We thank Lorenzo Marrucci for providing the q plates and the South African National Research Foundation for financial support.

APPENDIX: VECTOR NONSEPARABILITY

Here we outline the approach to modeling the observed behavior. Let U be expressed as a Jones vector in the horizontal-vertical basis, so that

$$U = \begin{pmatrix} \sqrt{\alpha}\exp(i\ell\phi) \\ \sqrt{1-\alpha}\exp(-i\ell\phi) \end{pmatrix},$$

which in the Dirac notation reads

$$|U\rangle = \sqrt{\alpha}|\ell, H\rangle + \sqrt{1-\alpha}|-\ell, V\rangle.$$

Now we assume that the action of the gain is to modify the modal weightings, so that the transfer matrix M may be written as

$$M = \begin{pmatrix} \sqrt{\eta_{h0}} & 0 \\ 0 & \sqrt{\eta_{v0}} \end{pmatrix},$$

where η_{h0} and η_{v0} represent intensity enhancements when the crystal is oriented at an initial angle $\theta = 0$. Now we rotate the crystal, transforming the input state to a new output state given by

$$\tilde{U} = R(\theta)MR(-\theta)U,$$

where $R(\theta)$ is the well-known rotation matrix. Thus,

$$\tilde{U} = \begin{pmatrix} \cos\theta & -\sin\theta \\ \sin\theta & \cos\theta \end{pmatrix}\begin{pmatrix} \sqrt{\eta_{h0}} & 0 \\ 0 & \sqrt{\eta_{v0}} \end{pmatrix}\begin{pmatrix} \cos\theta & \sin\theta \\ -\sin\theta & \cos\theta \end{pmatrix}U,$$

or

$$\tilde{U} = \begin{pmatrix} a_1\exp(i\ell\phi) + a_3\exp(-i\ell\phi) \\ a_2\exp(i\ell\phi) + a_4\exp(-i\ell\phi) \end{pmatrix},$$

which in Dirac notation reads

$$|\tilde{U}\rangle = a_1|\ell, H\rangle + a_2|\ell, V\rangle + a_3|-\ell, H\rangle + a_4|-\ell, V\rangle.$$

This is a pure state but not always separable. To calculate the purity, we first normalize the coefficients so that $\sum_i |a_i|^2 = 1$ and then calculate the purity from the density matrix of the state, ρ, following $V = \sqrt{1 - \mathrm{Tr}(\rho)}$ with

$\rho = |\tilde{U}\rangle\langle\tilde{U}|$, where Tr is the trace operator. This results in an analytical expression given by

$$V = 2|a_1 a_4 - a_2 a_3|,$$

with normalized coefficients, or

$$V = \frac{2|a_1 a_4 - a_2 a_3|}{\sum_i |a_i|^2},$$

for unnormalized coefficients, as it would be in the experiment. To find V experimentally, we determine a reduced form of the density matrix by performing a state tomography of the amplified beam [41,42]. This involves the following procedural steps: (i) Measure the overlap of $\tilde{U}_h$ with each of the six spatial projections given in Table I, i.e., two pure OAM modes and four superpositions following the known approach of optical inner products [15]; (ii) repeat this for the incoming state $\tilde{U}_v$. Note that $\tilde{U}_h$ and $\tilde{U}_v$ can be selected from $\tilde{U}$ by polarization optics as illustrated in the experimental setup, or alternatively all projections on each polarization component can be done in one step with a polarization grating and multiplexing setup [42]. The 12 measurements form a reduced tomography from which the nonseparability of a state may be calculated.

[1] Halina Rubinsztein-Dunlop *et al.*, Roadmap on structured light, J. Opt. **19**, 013001 (2017).

[2] Qiwen Zhan, Cylindrical vector beams: From mathematical concepts to applications, Adv. Opt. Photonics **1**, 1 (2009).

[3] Thomas G. Brown, Unconventional polarization states: Beam propagation, focusing and imaging, Prog. Opt. **56**, 81 (2011).

[4] B. Ndagano, I. Nape, M. A. Cox, C. Rosales-Guzman, and A. Forbes, Creation and detection of vector vortex modes for classical and quantum communication, J. Lightwave Technol. **36**, 292 (2018).

[5] Giovanni Milione, H. I. Sztul, D. A. Nolan, and R. R. Alfano, Higher-Order Poincaré Sphere, Stokes Parameters, and the Angular Momentum of Light, Phys. Rev. Lett. **107**, 053601 (2011).

[6] Giovanni Milione, S. Evans, D. A. Nolan, and R. R. Alfano, Higher Order Pancharatnam-Berry Phase and the Angular Momentum of Light, Phys. Rev. Lett. **108**, 190401 (2012).

[7] V. G. Niziev, R. S. Chang, and A. V. Nesterov, Generation of inhomogeneously polarized laser beams by use of a sagnac interferometer, Appl. Opt. **45**, 8393 (2006).

[8] Ting-Hua Lu and Y. C. Wu, Observation and analysis of single and multiple high-order Laguerre-Gaussian beams generated from a hemi-cylindrical cavity with general astigmatism, Opt. Express **21**, 28496 (2013).

[9] Darryl Naidoo, Filippus S. Roux, Angela Dudley, Igor Litvin, Bruno Piccirillo, Lorenzo Marrucci, and Andrew Forbes, Controlled generation of higher-order Poincaré sphere beams from a laser, Nat. Photonics **10**, 327 (2016).

[10] T. Grosjean, D. Courjon, and M. Spajer, An all-fiber device for generating radially and other polarized light beams, Opt. Commun. **203**, 1 (2002).

[11] M. Stalder and M. Schadt, Linearly polarized light with axial symmetry generated by liquid-crystal polarization converters, Opt. Lett. **21**, 1948 (1996).

[12] Lorenzo Marrucci, C. Manzo, and D. Paparo, Pancharatnam-Berry phase optical elements for wave front shaping in the visible domain: Switchable helical mode generation, Appl. Phys. Lett. **88**, 221102 (2006).

[13] Peng Chen, Wei Ji, Bing-Yan Wei, Wei Hu, Vladimir Chigrinov, and Yan-Qing Lu, Generation of arbitrary vector beams with liquid crystal polarization converters and vector-photoaligned q-plates, Appl. Phys. Lett. **107**, 241102 (2015).

[14] Wei Han, Wen Cheng, and Qiwen Zhan, Flattop focusing with full Poincaré beams under low numerical aperture illumination, Opt. Lett. **36**, 1605 (2011).

[15] Andrew Forbes, Angela Dudley, and Melanie McLaren, Creation and detection of optical modes with spatial light modulators, Adv. Opt. Photonics **8**, 200 (2016).

[16] Filippo Cardano, Ebrahim Karimi, Sergei Slussarenko, Lorenzo Marrucci, Corrado de Lisio, and Enrico Santamato, Polarization pattern of vector vortex beams generated by q-plates with different topological charges, Appl. Opt. **51**, C1 (2012).

[17] Christian Maurer, Alexander Jesacher, Severin Fürhapter, Stefan Bernet, and Monika Ritsch-Marte, Tailoring of arbitrary optical vector beams, New J. Phys. **9**, 78 (2007).

[18] Xiang Hao, Cuifang Kuang, Tingting Wang, and Xu Liu, Effects of polarization on the de-excitation dark focal spot in sted microscopy, J. Opt. **12**, 115707 (2010).

[19] L. Novotny, M. R. Beversluis, K. S. Youngworth, and T. G. Brown, Longitudinal Field Modes Probed by Single Molecules, Phys. Rev. Lett. **86**, 5251 (2001).

[20] Bienvenu Ndagano, Robert Brüning, Melanie McLaren, Michael Duparré, and Andrew Forbes, Fiber propagation of vector modes, Opt. Express **23**, 17330 (2015).

[21] Giovanni Milione *et al.*, 4×20 gbit/s mode division multiplexing over free space using vector modes and a q-plate mode (de) multiplexer, Opt. Lett. **40**, 1980 (2015).

[22] Alan E. Willner *et al.*, Optical communications using orbital angular momentum beams, Adv. Opt. Photonics **7**, 66 (2015).

[23] Alan E. Willner, Yongxiong Ren, Guodong Xie, Yan Yan, Long Li, Zhe Zhao, Jian Wang, Moshe Tur, Andreas F. Molisch, and Solyman Ashrafi, Recent advances in high-capacity free-space optical and radio-frequency communications using orbital angular momentum multiplexing, Phil. Trans. R. Soc. A **375**, 20150439 (2017).

[24] Valentina Parigi and Vincenzo D'Ambrosio, Christophe Arnold, Lorenzo Marrucci, Fabio Sciarrino, and Julien Laurat, Storage and retrieval of vector beams of light in a multiple-degree-of-freedom quantum memory, Nat. Commun. **6**, 7706 (2015).

[25] Cyril Hnatovsky, Vladlen G. Shvedov, Wieslaw Krolikowski, and Andrei V. Rode, Materials processing with a tightly focused femtosecond laser vortex pulse, Opt. Lett. **35**, 3417 (2010).

[26] Matthias Meier, Valerio Romano, and Thomas Feurer, Material processing with pulsed radially and azimuthally polarized laser radiation, Appl. Phys. A **86**, 329 (2007).

[27] O. J. Allegre, W. Perrie, S. P. Edwardson, G. Dearden, and K. G. Watkins, Laser microprocessing of steel with radially and azimuthally polarized femtosecond vortex pulses, J. Opt. **14**, 085601 (2012).

[28] A. A. Golyshev, A. M. Orishich, and V. B. Shulyatyev, Effect of the laser beam polarisation state on the laser surface quality, in *Proceedings of the Lasers in Manufacturing Conference* (Wissenschaftliche Gesellschaft Lasertechnik e.V. (WLT), 2015), p. 30, http://www.wlt.de/lim/Proceedings/Stick/PDF/Contribution175_final.pdf.

[29] Rudolf Weber, Andreas Michalowski, Marwan Abdou-Ahmed, Volkher Onuseit, Volker Rominger, Martin Kraus, and Thomas Graf, Effects of radial and tangential polarization in laser material processing, Phys. Procedia **12**, 21 (2011).

[30] André Loescher, Jan-Philipp Negel, Thomas Graf, and Marwan Abdou Ahmed, Radially polarized emission with 635 W of average power and 2.1 mJ of pulse energy generated by an ultrafast thin-disk multipass amplifier, Opt. Lett. **40**, 5758 (2015).

[31] Stefan Piehler, Xavier Délen, Martin Rumpel, Julien Didierjean, Nicolas Aubry, Thomas Graf, Francois Balembois, Patrick Georges, and Marwan Abdou Ahmed, Amplification of cylindrically polarized laser beams in single crystal fiber amplifiers, Opt. Express **21**, 11376 (2013).

[32] Fabien Lesparre *et al.*, High-power Yb : YAG single-crystal fiber amplifiers for femtosecond lasers in cylindrical polarization, Opt. Lett. **40**, 2517 (2015).

[33] R. J. C. Spreeuw, A classical analogy of entanglement, Found. Phys. **28**, 361 (1998).

[34] Andrea Aiello, Falk Töppel, Christoph Marquardt, Elisabeth Giacobino, and Gerd Leuchs, Quantum-like nonseparable structures in optical beams, New J. Phys. **17**, 043024 (2015).

[35] Diego Guzman-Silva, Robert Brüning, Felix Zimmermann, Christian Vetter, Markus Gräfe, Matthias Heinrich, Stefan Nolte, Michael Duparré, Andrea Aiello, Marco Ornigotti, and Alexander Szameit, Demonstration of local teleportation using classical entanglement, Laser Photonics Rev. **10**, 317 (2016).

[36] Falk Töppel, Andrea Aiello, Christoph Marquardt, Elisabeth Giacobino, and Gerd Leuchs, Classical entanglement in polarization metrology, New J. Phys. **16**, 073019 (2014).

[37] Stefan Berg-Johansen, Falk Töppel, Birgit Stiller, Peter Banzer, Marco Ornigotti, Elisabeth Giacobino, Gerd Leuchs, Andrea Aiello, and Christoph Marquardt, Classically entangled optical beams for high-speed kinematic sensing, Optica **2**, 864 (2015).

[38] L. J. Pereira, A. Z. Khoury, and K. Dechoum, Quantum and classical separability of spin-orbit laser modes, Phys. Rev. A **90**, 053842 (2014).

[39] W. F. Balthazar, C. E. R. Souza, D. P. Caetano, E. F. Galvao, J. A. O. Huguenin, and A. Z. Khoury, Tripartite nonseparability in classical optics, Opt. Lett. **41**, 5797 (2016).

[40] Bienvenu Ndagano, Benjamin Perez-Garcia, Filippus S. Roux, Melanie McLaren, Carmelo Rosales-Guzman, Yingwen Zhang, Othmane Mouane, Raul I. Hernandez-Aranda, Thomas Konrad, and Andrew Forbes, Characterizing quantum channels with non-separable states of classical light, Nat. Phys. **13**, 397 (2017).

[41] Melanie McLaren, Thomas Konrad, and Andrew Forbes, Measuring the nonseparability of vector vortex beams, Phys. Rev. A **92**, 023833 (2015).

[42] Bienvenu Ndagano, Hend Sroor, Melanie McLaren, Carmelo Rosales-Guzmán, and Andrew Forbes, Beam quality measure for vector beams, Opt. Lett. **41**, 3407 (2016).

[43] Lorenzo Marrucci, C. Manzo, and D. Paparo, Optical Spin-to-Orbital Angular Momentum Conversion in Inhomogeneous Anisotropic Media, Phys. Rev. Lett. **96**, 163905 (2006).

[44] Sergei Slussarenko, Anatoli Murauski, Tao Du, Vladimir Chigrinov, Lorenzo Marrucci, and Enrico Santamato, Tunable liquid crystal q-plates with arbitrary topological charge, Opt. Express **19**, 4085 (2011).

[45] Filippo Cardano, Ebrahim Karimi, Sergei Slussarenko, Lorenzo Marrucci, Corrado de Lisio, and Enrico Santamato, Polarization pattern of vector vortex beams generated by q-plates with different topological charges, Appl. Opt. **51**, C1 (2012).